Construction and Building Materials 367 (2023) 130282

Contents lists available at ScienceDirect

Construction and Building Materials

journal homepage: www.elsevier.com/locate/conbuildmat

Hardened oil well cement paste modified with TiO_2@SiO_2 nanoparticles: Physical and chemical properties

Giovanni dos Santos Batista [a], Antonio Shigueaki Takimi [b], Eleani Maria da Costa [a,*]

[a] School of Technology, Pontifical Catholic University of Rio Grande do Sul, 6681 Ipiranga Avenue, Building 30, Room 111/F, 90619-900 Porto Alegre, RS, Brazil
[b] School of Engineering, Federal University of Rio Grande do Sul, 9500 Bento Gonçalves Avenue, Building 43427, Room 216, 91501-970 Porto Alegre, RS, Brazil

ARTICLE INFO

Keywords:
Core/shell
Nanoparticle dispersion
Hydration
Oil well cement paste
Microstructure
Polycarboxylate

ABSTRACT

Core/shell TiO_2@SiO_2 nanoparticles (nTS) were added to cement class G, and their physical and chemical properties were investigated with and without polycarboxylate (PC). The hardened cement pastes were analyzed through gas pycnometry, Brunauer-Emmett-Teller (BET), field emission scanning electron microscopy (FE-SEM), and compressive strength. For hydration characterization, portlandite quantification, and C—S—H analysis, X-ray diffraction (XRD), Fourier transform infrared spectroscopy (FTIR), thermogravimetric analysis (TGA), and ^{29}Si magic-angle spinning nuclear magnetic resonance (^{29}Si MAS NMR) were performed. The nTS demonstrated a self-dispersive behavior and increased the specific mass and matrix compacity. Moreover, the total pore volume decreased, and the compressive strength increased. The nTS improved the hydration degree, reduced portlandite content, and increased C—S—H main chain length.

1. Introduction

The demand for new materials and blends with improved properties to be used as supplementary cementitious material (SCM) is increasing [1–4]. Currently, nanoparticles (NPs) have received great attention as SCM since they can improve the performance and durability of cement-based materials. Some examples of NPs that have been added to cementitious materials are silicon oxide (SiO_2) [5,6], aluminum oxide (Al_2O_3) [7], titanium oxide (TiO_2) [8], iron oxide (Fe_2O_3) [9,10], carbon nanotubes (CNTs) [11,12], graphene oxide (GO) [13,14] and clays [15–17]. The use of nanomaterials for oil well cementing is very promising since nanoparticles can modify some properties, such as rheology, heat of hydration, mechanical resistance, microstructure, shrinkage, and chemical resistance [18–20]. The addition of nanosilica (n-SiO_2) in concrete is widely reported, but its addition in oil-well cement is relatively scarce [21–23]. The main advantages of using n-SiO_2 are: creation of additional calcium-silicate-hydrate (C—S—H) nucleation points, accelerating hydration; reduction of calcium hydroxide (CH) and ettringite (AFm) crystal size, resulting in a more uniform C—S—H matrix; increase the pozzolanic activity, consuming CH to form additional C—S—H; free water immobilization, filling the voids between the cement grains; enhancement of the bonding between the aggregates and the cement paste [24].

On the other hand, adding non-reactive nanoparticles as a filler to oil-well cement is also interesting once they modify the hydration reaction due to dilution, alter the particle size distribution, changing the porosity, and provide additional sites for nucleation of the cement hydration products [25,26]. TiO_2 is an interesting material due to its chemical stability, low price, nontoxicity, and photocatalytic activity, which can impart biocidal, self-cleaning, and smog-abating functionality to cement-based materials [27]. When added to Portland cement, TiO_2 is considered an inert filler that modifies its properties, increasing C—S—H nucleation and compactness, not reacting with the matrix [28,29].

Blended additions using pozzolanic and inert SCMs have received attention, making it possible to take advantage of the properties of both materials, providing enhanced properties for the cement paste in fresh and hardened states. In the case of an oil well, the mechanical and chemical properties and durability of cement paste are very important since it is subjected to mechanical loading, temperature variation, interstitial pore pressure changes, and chemical attacks, such as CO_2 and H_2S [30]. Previously, studies using blends addition such as fly ash and zeolites [31], nanosilica and polymers [32,33], and graphene oxide and nanosilica [34] demonstrated the benefits of using more than one type of material. For example, the study of Xiao *et al.* [35] showed that the use of both nano-SiO_2 and nano-TiO_2 acting together is very promising. The early and later properties of ordinary cement paste, such as hydration

* Corresponding author.
E-mail address: eleani@pucrs.br (E.M. Costa).

https://doi.org/10.1016/j.conbuildmat.2022.130282
Received 24 October 2022; Received in revised form 6 December 2022; Accepted 29 December 2022
Available online 3 January 2023

rate, total pore volume, and compressive strength were improved when both nanoparticles were added [35]. However, besides the use of nanoparticle blends and their influence in cement class G properties were not reported in the literature, studies are still needed to develop better dispersive methods once blends have high tendency to agglomerate.

The production of core/shell materials gained attention at the beginning of the 21st century, but its application in cementitious materials began only in 2017 [36,37]. Therefore, there are still scarce studies on using these nanoparticles in cement-based materials as nano-SiO_2-coated TiO_2, also called core/shell TiO_2@SiO_2 (nTS). In the best of our knowledge, no one involving oil well cement. Han *et al.* [36] studied the application of core/shell in Portland cement mortar and coated TiO_2 rutile phase with SiO_2. They observed that the CH crystal size was reduced, and density and fracture toughness of the cement mortars were improved. Sun *et al.* [37] also added nTS to ordinary cement paste and observed a similar behavior. The microstructure became denser through nucleation and pozzolanic effects during cement hydration.

Despite what has been presented so far and all the advantages of nTS, it still follows the lack of studies related to the dispersion, microstructure, and chemical changes promoted by these nanoparticles. The self-dispersive property is an important and promising aspect related to nanoparticles since agglomeration harms their effect in cement-based materials. In this context, this study aims to investigate the physical and chemical properties of cement class G with addition of nanoparticles (nTS) with and without polycarboxylate as an advanced material to be used in critical conditions of operation in oil and gas industry. Furthermore, the physical and chemical changes promoted by nTS addition, such as pore refinement, mechanical resistance, portlandite content, hydration degree, and CSH main chain length were evaluated.

2. Materials and methods

2.1. Materials

The API Portland cement class G for oil well was supplied by Lafarge Holcim Brasil S.A. The nTS was acquired from SkySpring nanomaterials. It consists of 99.5 % purity rutile phase titanium oxide (TiO_2) nanoparticles coated with silicon oxide (SiO_2). The SiO_2/TiO_2 ratio is approximately 0.03, the nanoparticle size is between 20 and 40 nm, and this material is highly hydrophilic. The transmission electron microscopy (TEM) image and the thermogravimetric analysis (TGA) of nTS are shown in Fig. 1. As nTS reduces the cement workability, its behavior was tested with CQ Plast MR 825 addition, an ether polycarboxylate plasticizer (PC) of the third generation, provided by Camargo Química. The properties of the materials are shown in Table 1. The chemical composition of the cement and nTS are presented in Tables S1 and S2 of the Supplementary material.

Table 1
nTS, cement class G, and PC properties.

Material	Particle size	Density (g. cm^{-3})	Type	pH	Specific surface area ($m^2.g^{-1}$)
nTS	20–40 nm	4.25	Powder	N/A	> 40
Cement Class G	7.30 μm*	2.80–3.20	Powder	12–14	0.82*
PC	N/A	1.07–1.09	Liquid	4–6	N/A

*Determined by BET.

2.2. Cement slurries preparation

Before the mixing, the nTS was added to deionized water, and the mixer was set to a speed rotation of 2,000 rpm for 2 min. The correct weight of nTS was added to deionized water, respecting the 10A specification of the American Petroleum Institute (API) [38]. For 600 g of cement, the water/binder (w/b) ratio was 0.44. In the mixtures with PC addition, the w/b was reduced to 0.35. Two nTS amounts (0.5 and 1 wt % of cement) were chosen based on previous studies once a higher NPs amount causes particle agglomeration, deleterious to the properties of cementitious material [23,39]. The PC amount was 0.15 wt% of cement. The composition of each cement mixture is specified in Table 2. Dynamic Light Scattering (DLS) was carried out in a ZEN3600 equipment from Malvern Panalytical to investigate particle dispersion in water and in the presence of PC. The 1nTS and 1nTS-PC mixtures were tested without cement, and the results are presented in Fig. 2. When the w/b ratio is 0.44, the nTS offered an excellent dispersion, with a Z-average diameter of 32.66 nm. When the w/b is reduced to 0.35 and the PC is added, the Z-average diameter increased to 57.81 nm. This indicated that lower water content and additive addition contributed to particle agglomeration.

The cement pastes preparation started immediately after the nTS mixing with water, following the API 10A specification [38]. The mixer (Model 7000 Constant Speed from Tulsa) was set to a rotation of 4,000 rpm for 15 s for the cement addition and 12,000 rpm for 35 s for complete homogenization. A cylindrical polyvinyl chloride (PVC) mold of

Table 2
Composition of the cement pastes.

Mixtures	Cement (g)	Water (mL)	nTS (g)	PC (g)
REF	600	264	–	–
0.5nTS	600	264	3.0	–
1nTS	600	264	6.0	–
REF-PC	600	210	–	0.9
0.5nTS-PC	600	210	3.0	0.9
1nTS-PC	600	210	6.0	0.9

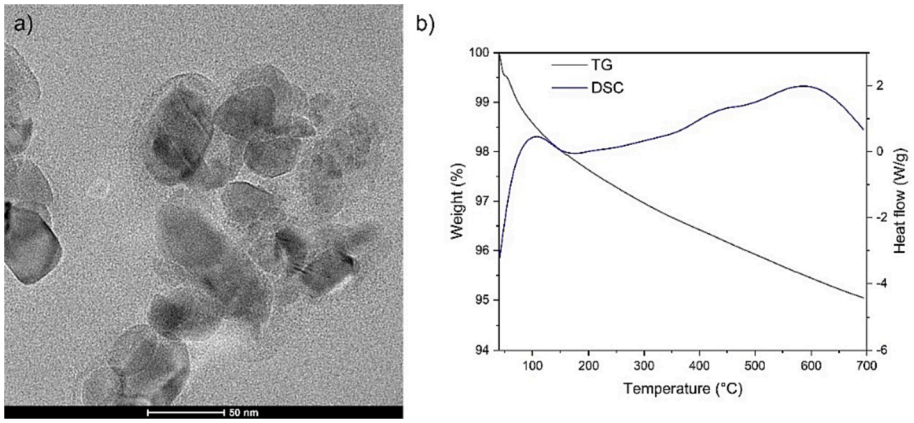

Fig. 1. (a) TEM image and (b) TGA thermogram of nTS nanoparticles.

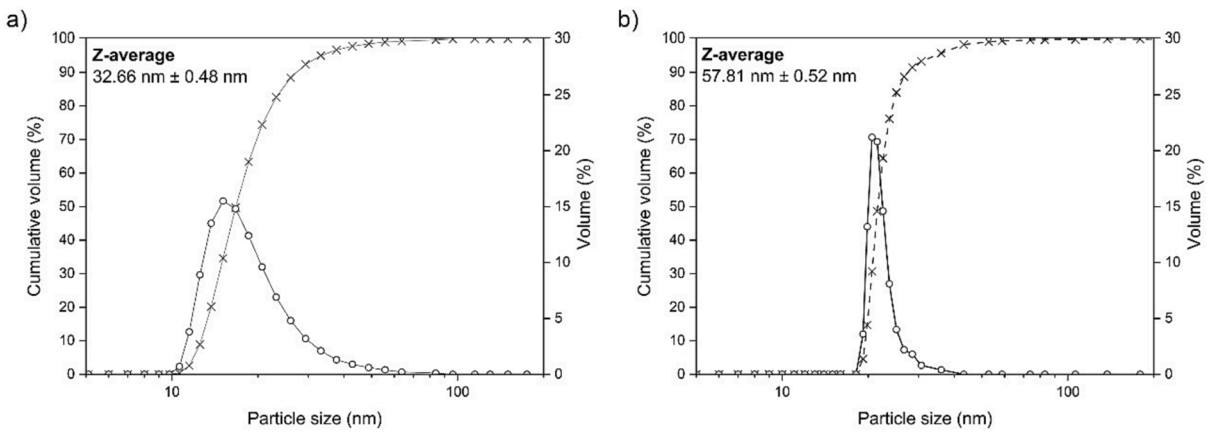

Fig. 2. DLS results from (a) 1nTS and (b) 1nTS-PC.

120 mm height and 21.6 mm diameter was used to produce the specimens. The slurry was poured into the mold in two layers with 20 strokes per layer using a 3 mm diameter metal rod. For the initial cure of specimens, the molds were immersed in deionized water inside a pressure vessel, heated at 60 °C, and pressurized at 4 MPa with nitrogen (N_2) for 4 h. The specimens were demolded and cut with a Buehler Isomet low-speed precision saw to 43.2 mm height. Then, the specimens underwent to additional cure process in deionized water for 20 h at 60 °C to guarantee the maximum percent of hydration products in 24 h [40]. A new cement slurry was made for each paste composition.

2.3 Characterization of the specimens

2.3.1. Nitrogen gas pycnometry

Nitrogen gas pycnometry was used to measure the hardened cement paste density variations with nTS addition. Prior the measurements, the cylindrical specimens were oven-dried under vacuum at 60 °C for 7 days to complete water removal. The analysis was performed in triplicate in a Quantachrome Multipycnometer equipment with N_2 gas.

2.3.2. Pore volume and pore size determination

The Brunauer-Emmet-Teller (BET) analyses were carried out to quantify total pore volume and pore size differences in the cementitious matrix due to nTS addition. Before analysis, the samples were cut into small pieces and oven-dried under vacuum at 60 °C for 7 days for water removal. After that, the samples were degassed with N_2 in the FlowPrep 060 equipment for 24 h and analyzed in the Tristar II Plus equipment from Micromeritics, with N_2 gas, filler rod, and nitrogen bath (−195.85 °C). The analysis was performed in triplicate for each cement paste mixture.

2.3.3. Microstructure characterization

The FE-SEM was used to observe the matrix microstructure and density differences as nTS was added. The analyses were carried out in a FEI Inspect F50 model microscope. For the microstructure examination, the specimens were cut in slices, grounded with SiC sandpaper from #220 to #1200, and polished with alumina 1 and 0.3 μm, respectively. The surface was covered with a thin gold film to become conductive. The images were acquired using secondary electron (SE) mode.

2.3.4. Compressive strength tests

The compressive strength tests were performed to evaluate the influence of nTS on cement paste mechanical resistance. The cured specimens were capped with sulfur for surface regularization. Three specimens per mixture were tested in an EMIC PC200I model using a constant speed deformation of 1 mm/min, following the C39/C39M-21 [41] specifications.

2.3.5. X-ray diffraction (XRD)

The XRD technique was used to identify crystalline phases, such as CH, C_3S, and C_2S, as nTS was added. The powder was obtained by grinding the cured cement paste specimens with a mortar and pestle. A Bruker D8 Advance A25 powder diffractometer with Cu Kα radiation (λ = 1.5406 Å), a voltage of 40 kV, a current of 30 mA, a step of 0.015°, a scan interval of 10-80° 2θ, and a split of 0.6 mm were used.

2.3.6. Fourier transform infrared spectroscopy (FTIR)

The FTIR analysis was performed to observe changes with nTS addition in –OH stretching vibrations of CH, CO_3^{2-} stretching vibration of carbonate groups ($CaCO_3$), and C—S—H formation and its polymerization. After the curing, the powder sample was obtained by grinding the cement paste specimens with a mortar and pestle. The spectra were recorded in a PerkinElmer Spectrum 3 equipment using the Attenuated Total Reflectance (ATR) accessory. The wavenumber range was set from 4000 to 650 cm^{-1}, and 12 scans were performed per sample.

2.3.7. Thermogravimetric analysis (TGA)

The TGA analysis was used to investigate the hydration product formation differences with nTS addition. After the curing, the powder sample was obtained by grinding the hardened cement specimens with a mortar and pestle. Minor chemical changes are detected through this method. The analyses were performed in the STD 650 equipment from TA instruments using N_2 gas and a heating rate of 10 °C/min from 40 to 1000 °C.

2.3.8. ^{29}Si magic angle spinning – nuclear magnetic resonance (^{29}Si MAS NMR)

Solid-state ^{29}Si MAS NMR was performed to observe chemical shifts of silicon tetrahedron as a consequence of nTS addition. Furthermore, the hydration degree of cement silicate minerals (α_c) and C—S—H mean chain length (MCL) were quantified using Eqs. (1) and (2), respectively. For this analysis, the powder sample was obtained by grinding the hardened cement specimens with a mortar and pestle. The analyses were carried out in triplicate using an Avance III 400 MHz equipment from Bruker. The number of scans was 60,000. The magnetic field strength, the resonance frequency, and the magic angle rotation were 9.4 T, 79.4 MHz, and 5 kHz, respectively. The pulse width was 4 μs, and the cycle time was 5 s. The spectra were deconvoluted with Bruker TopSpin® 4 software.

$$\alpha_c = 1 - \frac{Q^0}{Q_0^0} \tag{1}$$

where: Q^0 is the percentage of silicate tetrahedra in hydrated cement; Q_0^0 is the percentage of silicate tetrahedra in anhydrous cement.

$$MCL = \frac{Q^1 + Q_p^2 + 1.5Q_b^2}{0.5Q^1} \quad (2)$$

where: Q^1, Q_p^2, and Q_b^2 are the percentages of C—S—H silicate tetrahedra in hydrated cement.

3. Results and discussion

3.1. Physical, microstructural, and mechanical properties

The gas pycnometry results of the cured specimens with and without nTS are presented in Fig. 3. The REF specimen showed a specific mass value of 2.24 $g.cm^{-3}$. When 0.5 wt% of nTS was added, the specific mass decreased by approximately 5 %, reaching a value of 2.13 $g.cm^{-3}$. However, with the nTS content increase from 0.5 wt% to 1 wt%, the specific mass slightly increased, being only 2 % higher than the REF (2.28 g/cm^3).

In general, the specimens with PC exhibited a higher specific mass than those without additive. The specific mass of the REF-PC and 0.5nTS-PC specimens were 2.29 and 2.52 $g.cm^{-3}$, respectively, which corresponds to an increase of 10 % in presence of 0.5 wt% of nTS. However, a reduction on the specific mass was found for the higher content of nTS (1 wt%), but its specific mass value (2.34 $g.cm^{-3}$) is still higher than the REF-PC by approximately 2 %.

Batista *et al.* [23] also found an increase in specific mass after adding 1 wt% of 50 nm n-SiO_2 to cement class G. The increase was around 1.40 %. The reason for this behavior was the filler and pozzolanic effects of n-SiO_2. However, the authors reported that when the nanoparticle content was raised, a reduction in specific mass occurred due to particle agglomeration [23]. The specific mass reduction noted in our study was much more pronounced, probably due to the better dispersion and smaller particle size of nTS.

Total pore volume and average pore diameter were determined through the BET technique to better know the nTS effects. The results are presented in Fig. 4. The total pore volume values agree with the specific mass results. Values of 0.0342, 0.0379 (+10.8 %) and 0.0283 $g.cm^{-3}$ (–33.9 %) were found for the REF, 0.5nTS and 1nTS, respectively.

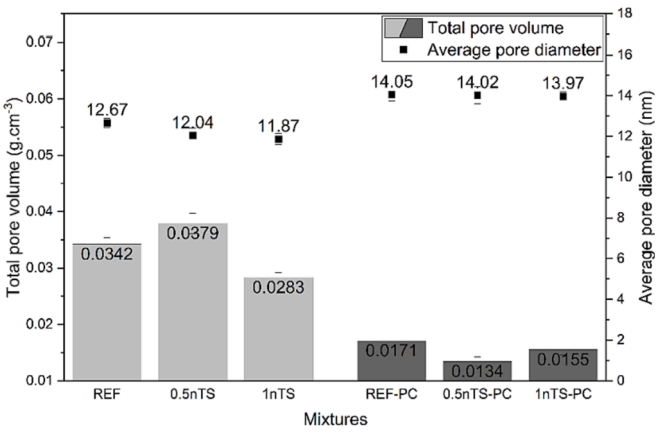

Fig. 4. Total pore volume and average pore diameter.

The high pore volume observed in 0.5nTS specimen can explain the low specific mass, previously identified for this mixture. The total pore volume significantly reduced when the nTS content was 1 wt%. In the PC presence, the total pore volume values were lower when compared with the specimen without additive. The REF-PC, 0.5nTS-PC, and 1nTS-PC showed values of 0.0171, 0.0134 (−27.6 %), and 0.0155 (−10.3 %) $g.cm^{-3}$. The average pore diameter was higher for the mixtures with PC but presented no significant variation as nTS was added. After adding 1 wt% of nTS with 15–20 nm to ordinary cement paste with a w/s ratio of 0.50, Sun *et al.* [42] also noticed a reduction in the average capillary pores using Mercury Intrusion Porosimetry. The total porosity decreased by 14.47 % compared to the reference. However, the less pronounced decrease found by the authors when compared to our study could be related to the characterization technique and the sample preparation that were performed.

The nTS effects in the microstructure are shown in the FE-SEM images presented in Fig. 5. A more homogeneous and compact microstructure is formed when nTS is present due the filler effect and because the nTS particles provide extra sites for C—S—H nucleation. This

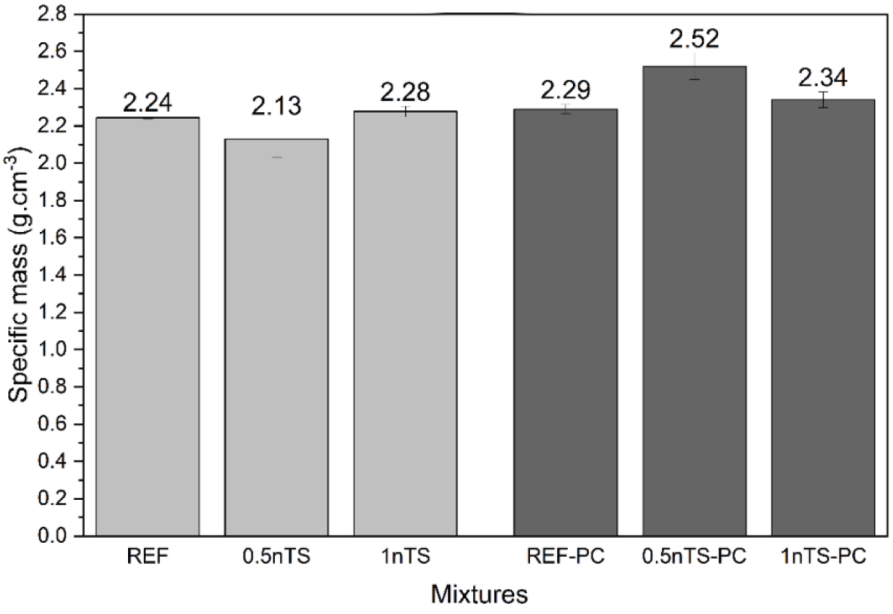

Fig. 3. Specific mass of the specimens.

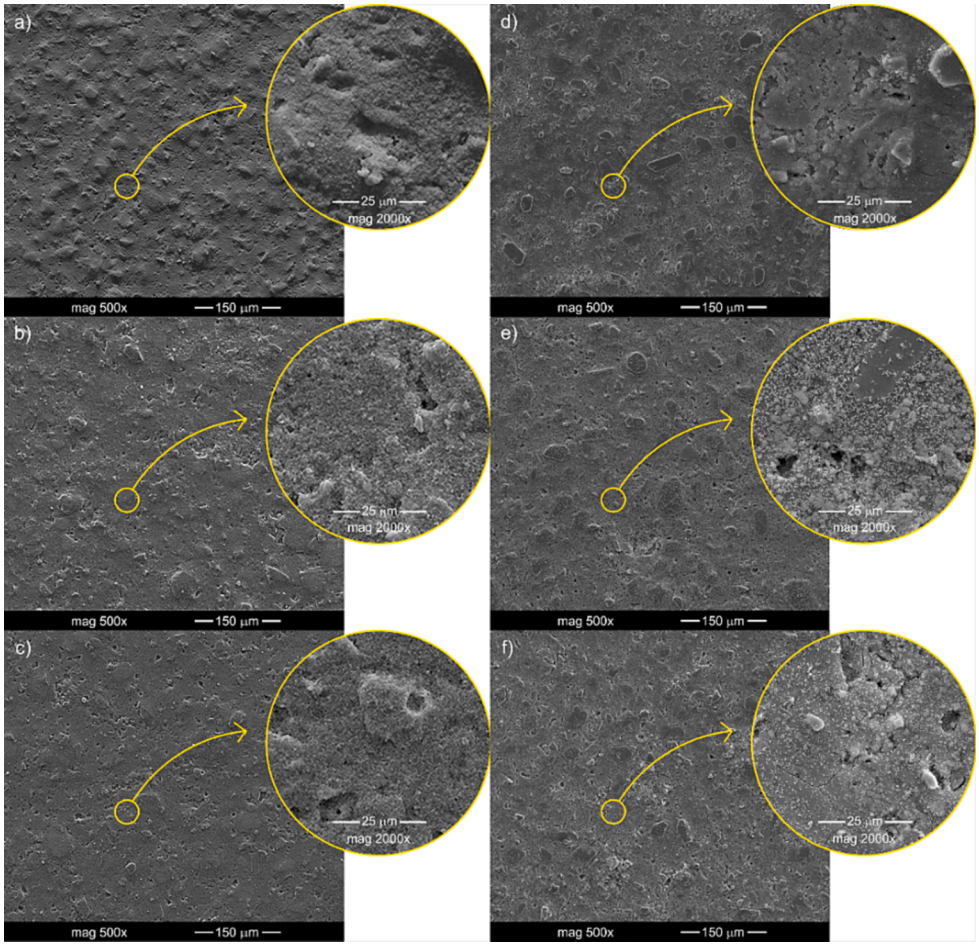

Fig. 5. FE-SEM images of the hardened cement paste microstructure. (a) REF, (b) 0.5nTS, (c) 1nTS, (d) REF-PC, (e) 0.5nTS-PC, and (f) 1nTS-PC.

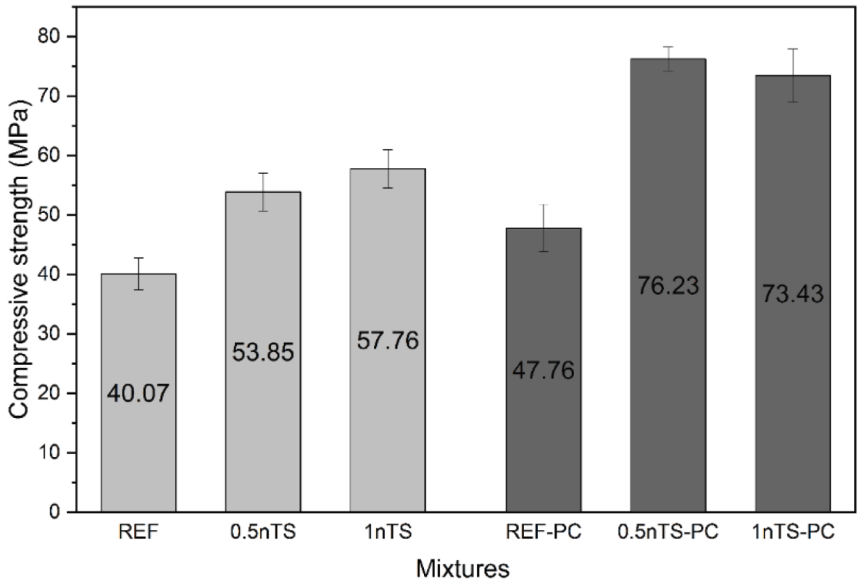

Fig. 6. Compressive strength tests of the specimens.

observation agrees with the BET results, in which the total porosity has decreased when nTS was added. The improvement in the microstructure densification is more evident for the 1nTS cement paste, as shown in Fig. 3c. Furthermore, the microstructure became denser after reducing the w/b ratio to 0.35 and adding PC. This effect was expected and have been reported by some authors in cement-based materials with addition of PC [43–46]. The specimens with nTS and PC addition presented a more homogeneous microstructure probably due to the w/b reduction, consequently increasing cohesion. However, no significant changes in microstructure were observed between 0.5nTS-PC and 1nTS-PC specimens. Analogous effects were observed by Han *et al.* [36] when added 1, 3, and 5 wt% of 20 nm NSCT to cement mortar, both CH crystal size and CH amount were reduced with nanoparticle addition. In other similar study, after adding 1 wt% of 10–15 nm nTS to ordinary cement paste, Sun *et al.* [37] also noticed a much denser and more compact microstructure. Moreover, a higher content of hydrates was found with nTS addition. Both authors concluded that this happens due to the pozzolanic, and C—S—H nucleation effects caused by the SiO_2 shell and TiO_2 core, respectively.

Compressive strength test results are shown in Fig. 6. The REF, 0.5nTS, and 1nTS specimens presented compressive strength average values of 40.07, 53.85, and 57.76 MPa, respectively. The compressive strength increased with increasing content of nTS, 34.4 and 44.1 % for the 0.5nTS and 1nTS, respectively, compared to the REF. This behavior was predictable since a denser microstructure was observed for the samples with nTS addition. The REF-PC specimen exhibited a higher compressive strength average value (47.76 MPa) compared with REF paste without PC (40.07 MPa). The PC effect on compressive strength increase was expected, which was already stated by some authors [47,48]. When 0.5 wt% of nTS was added, the compressive strength presented a remarkable increase reaching a value of 76.23 MPa, which corresponds an increasing of 59.6 %. However, the average compressive strength value for the 1nTS-PC specimen (73.43 MPa) remained almost the same than the 0.5nTS-PC. As shown in FE-SEM images of Fig. 5, by comparing the microstructures of 0.5nTS-PC and 1nTS-PC cement pastes no significant differences can be identified. This can be related to the water content reduction favoring nTS particles agglomeration, as previously revealed by DLS analysis (Fig. 2). The compressive strength values obtained with nTS addition were very satisfactory compared to those reported by the literature for oil well cement.

After adding 1 wt% of 20 nm NSCT to mortar, Han *et al.* [36] found a compressive strength increase of 5.97 % when compared to the reference specimen. With 1 wt% of 10–20 nm nTS addition to ordinary cement paste, Sun *et al.* [37] observed a compressive strength increase of 10 %. The increase in compressive strength was attributed to the filler and pozzolanic activities of nanoparticles, reacting with CH while hydration products are formed, thereby increasing nucleation and matrix densification. The compressive strength increase observed in our study was expressively superior, approximately 44.15 % for the 1nTS mixture. This is probably related to a better dispersion and higher pozzolanic reaction of nTS improving the microstructure of oil well cement paste.

3.2. Portlandite quantification and hydration degree

For further investigation of the pozzolanic effect, CH consumption, and secondary C—S—H formation due to nTS addition, XRD, FTIR, TGA, and ^{29}Si MAS NMR were performed.

Fig. 7 shows the XRD spectra of the samples. Calcium hydroxide (CH), calcium carbonate (C), tricalcium silicate (C_3S – A), and dicalcium silicate (βC_2S – B) are the main compounds identified through XRD

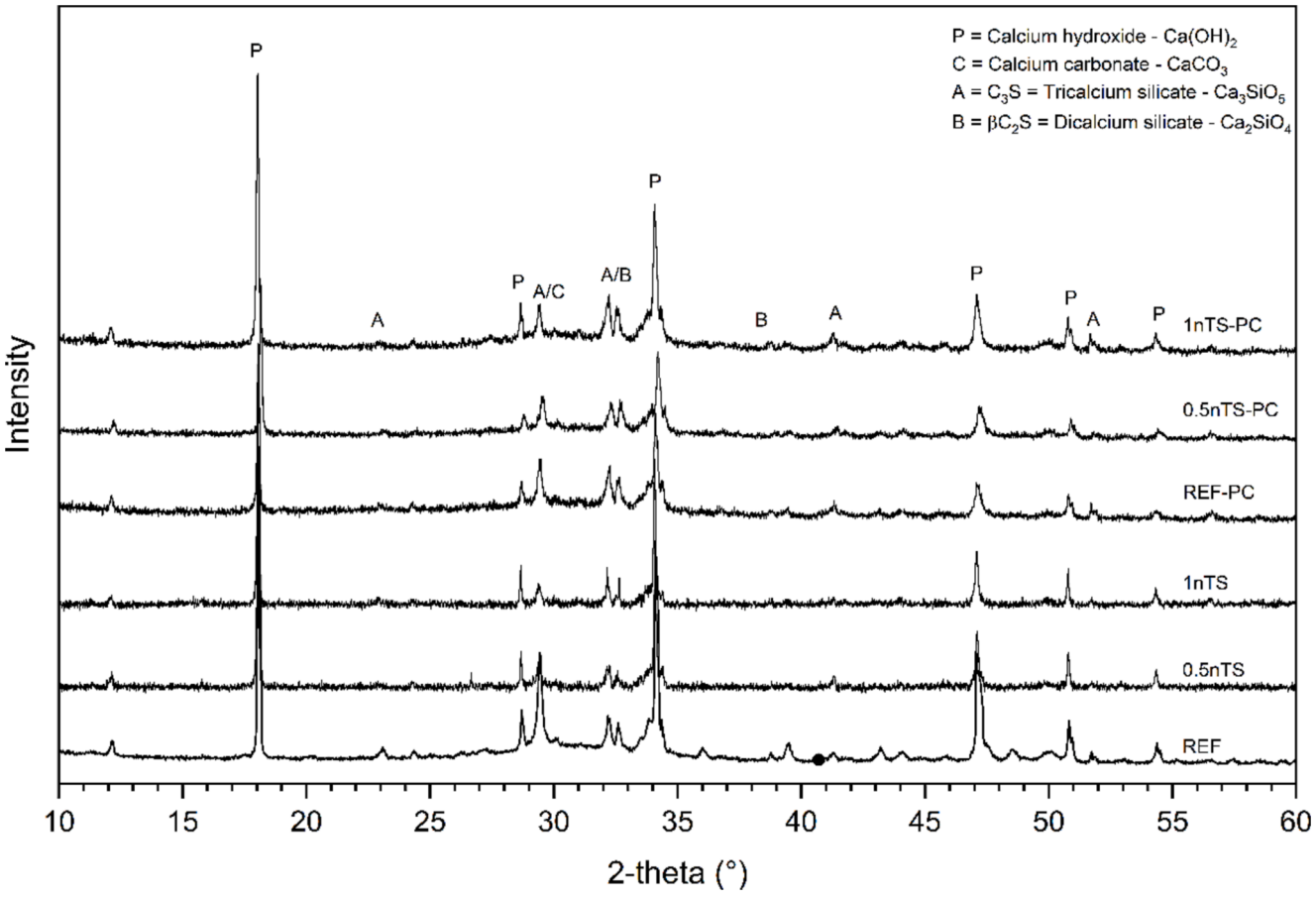

Fig. 7. XRD spectra of the samples.

analysis. The presence of calcium carbonate is related to natural carbonation [49]. The CH peaks presented a remarkable intensity reduction as nTS was added, indicating CH consumption due to the pozzolanic effect and increase of C—S—H nucleation sites. On the other hand, for the samples with PC addition, the portlandite peak decreased for the 0.5nTS-PC mixture but increased for the 1nTS-PC. This increase is probably related to particle agglomeration due to high nTS addition, previously detected by DLS. A similar behavior was also observed for the calcium silicate peaks (A and B), which were reduced as nTS was added. Less content of unhydrated compounds was found in nTS samples. This is associated with a higher hydration rate and pozzolanic effect due to nTS addition. However, when PC was added, the intensity of calcium silicate peaks was even higher than the REF mixture, indicating higher content of unhydrated products. This effect is the retardation of hydration (mainly on C_3S reaction) caused by superplasticizer addition during the first 30 h and was already reported by many authors [50–52]. In the study of Sun *et al.* [42], 1 wt% of nTS was added to cement paste, and a very similar behavior was noticed. Both calcium hydroxide and silicate peaks were reduced, evidencing the increase of hydration rate and pozzolanic effect of nTS, in agreement with the results found in our study. FTIR, TG, and NMR were performed for additional investigations related to CH consumption and unhydrated products.

The FTIR spectra of the samples are presented in Fig. 8. The sharp band at 3641 cm^{-1} is attributed to the –OH stretching vibrations in CH [53,54]. The broad bands observed from 3600 to 3000 cm^{-1} and centered at 1641 cm^{-1} are related to stretching and bending vibrations of –OH in water [55,56]. With nTS addition, a decrease on the intensity of the peaks related to –OH is noticed, indicating less CH and free water quantities. A similar behavior is observed when the w/b is reduced, and the PC is added. When the nTS content was increased from 0.5 to 1 wt% (1nTS-PC), the peak became sharper, associated with increasing in the CH content probably related to particle agglomeration. To quantify the CH content, TG analysis was performed.

The wide band observed between 1600 and 1300 cm^{-1} represents the asymmetric CO_3^{2-} stretching in carbonate ($CaCO_3$) groups. Two peaks characterize this region. The higher band region (1472 cm^{-1}) indicates the presence of vaterite/aragonite, while the lower band region (1417 cm^{-1}) corresponds to calcite. The sharp band located at 874 and 712 cm^{-1} are related to out-of-plane and in-plane vibrations of CO_3^{2-} [53,57]. As previously detected by XRD, $CaCO_3$ was formed through the natural carbonation of CH during the sample preparation and storage.

The band between 964 and 961 cm^{-1} is attributed to Si-O stretching vibrations of C—S—H presence [54,58,59]. This band narrowed with nTS and PC addition. In addition, a slight shift to the left was observed for the samples containing nTS and PC. This was due to a C—S—H with a higher order structure. Furthermore, the intensity of the band located at approximately 920 cm^{-1} is reduced as nTS is added, indicating consumption of the anhydrous cement phases (C_3S and C_2S) and consequently increase in hydration degree. These results agree with XRD analyses, reinforcing the increase of nucleation sites and the pozzolanic effect of nTS. To better understand the hydration degree and C—S—H formation, NMR analysis was carried out.

The TGA thermograms of the samples are presented in Fig. 9, showing three characteristic regions of mass loss at 115, 450–600, and 650 °C. The first region, located at 115 °C, is related to free water removal and dehydration from cement hydration products, such as C—S—H and ettringite [60,61]. The inflection at 450–600 °C, which shows a high mass loss variation, is related to CH decomposition [62,63]. The weight loss in this region was 4.838 and 3.183 % for the REF and 1nTS, respectively. The weight loss percentage decreases in presence of nTS, indicating CH reduction due to the nanoparticle pozzolanic effect. No significant difference was observed for the samples with PC addition, being 4.148 and 3.934 % of weight loss for the REF-PC and 1nTS-PC, respectively. After adding 1 wt% of nTS to Portland cement paste, Sun et al. [42] observed a decrease in CH content from 7.13 to 6.31 % after 3 days of curing. The CH reduction found in our study (1.66 %) was twice the value found by Sun et al. [42] (0.82 %). Many factors could be explained the differences, such as particle size, surface area and curing method. In this work the cement pastes were cured at 60 °C temperature influencing the CH formation and consumption related to pozzolanic reactions [64]. The weight variation at approximately 650 °C is associated with calcium carbonate decomposition [65,66]. The $CaCO_3$ appearance is due to the natural carbonation

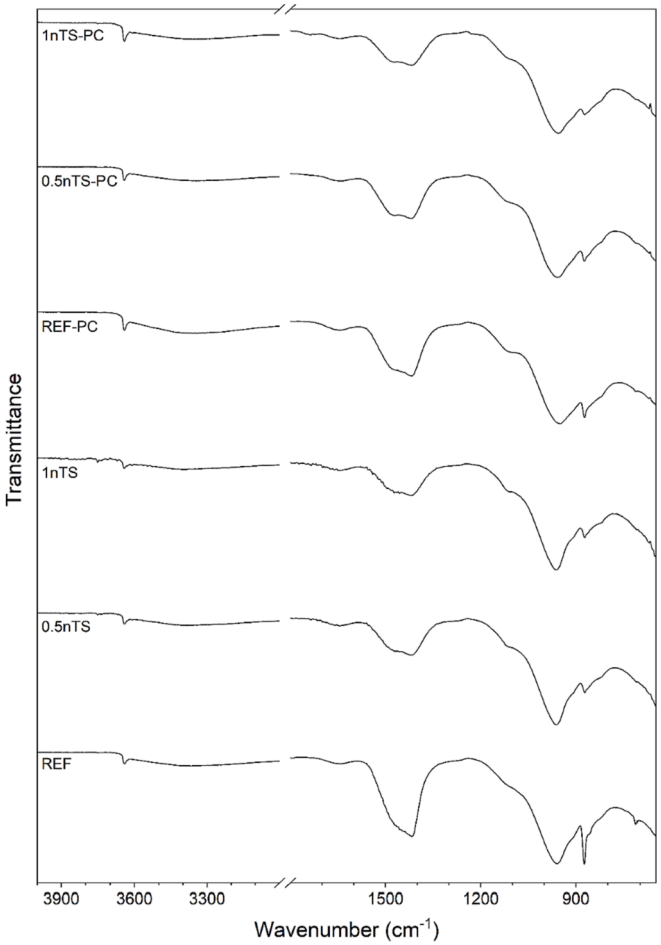

Fig. 8. FTIR spectra of the samples.

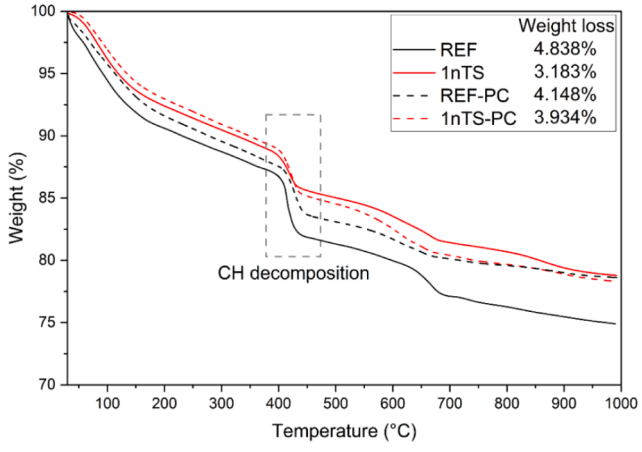

Fig. 9. TGA thermograms of the samples.

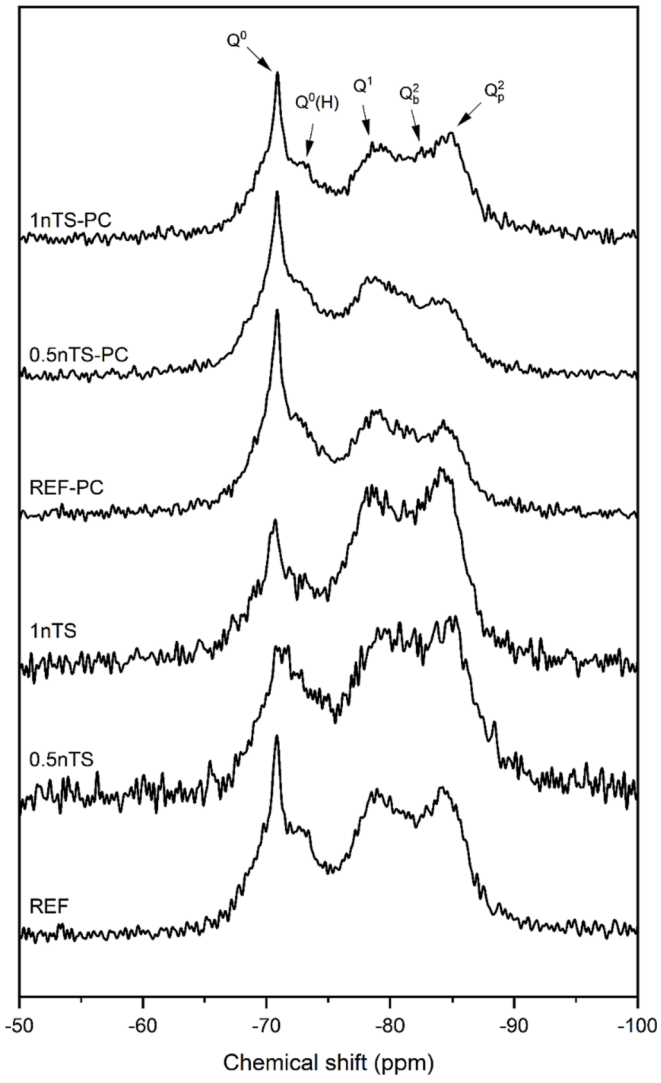

Fig. 10. ^{29}Si MAS NMR spectra of the samples.

during the sample preparation. The TGA results agree with those revealed by XRD and FTIR analyses.

^{29}Si MAS NMR spectra are presented in Fig. 10, demonstrating changes in C—S—H microstructure with nTS addition. The peak position, percentage area of the deconvoluted components, hydration degree, and the C—S—H MCL are given in Table 3. The Q^0 and Q^0 (1H) signals are related to residual anhydrous clinker phases (C_3S and C_2S). In presence of nTS, the Q^0 intensity (at −71 and −73 ppm) decreases, indicating a higher hydration degree. The α_c quantitively represents the cement hydration degree. Hydration values of 41.46, 49.42, and 56.64 % were found for the REF, 0.5nTS, and 1nTS samples, respectively. The hydration difference between the REF and the 1nTS sample was 15.18 %. This increase in the hydration rate is directly related to the increase in the hydration degree. Han et al. [36] and Sun et al. [42] also observed an increase in hydration using NSCT and nTS, but in lower levels. After curing the samples for 3 d and adding 1 wt% of NSCT, Han *et al.* [36] reached a hydration degree increase of 2.21 % compared to the reference sample and increased to 5.20 % with 5 wt% of NSCT. When adding 1 wt% of nTS, Sun *et al.* [42] found a hydration rate 5.91 % higher than the reference sample. The higher value found by our study can be related to a better particle dispersion and due to the different curing method, which improve the hydration reactions. However, the samples with a lower w/b ratio and PC presented a relatively lower hydration degree. Values of 37.18, 36.46, and 46.71 % were found for the REF-PC, 0.5nTS-PC, and 1nTS-PC, respectively. The first two samples exhibited a lower hydration degree than the REF (41.46 %). This retardation effect (mainly on alite reaction) caused by superplasticizer addition during the first 30 h of hydration is already known and reported by many authors [50–52].

The Q^1, Q^2_b, and Q^2 signals are related to typical C—S—H gel [67]. A Q^1 with a higher relative intensity than Q^2_b means C—S—H formation with a short MCL [68]. In addition, the increase in the Q^2/Q^1 ratio implies a reduction in the Ca/Si ratio [69]. The Q^1, Q^2_b, and Q^2_P signals were located at −78, −81, and −84 ppm, respectively. The Q^2/Q^1 ratio and MCL changed with nTS addition. The REF sample showed a Q^2/Q^1 ratio of 1.48, while the 0.5nTS and 1nTS presented 1.61 and 1.65, respectively, indicating an increase in the Ca/Si ratio with nTS addition. Furthermore, an MCL increment from 5.35 (REF) to 5.75 (0.5nTS), and then 5.80 (1nTS) was observed. This MCL rise led to a higher C—S—H polymerization. The increased MCL elongation and packing of silicate chains were suggested to stiffen the material, enhancing the compressive strength [69].

However, the samples with lower w/b ratio and PC addition decreased both Q^1/Q^2 ratio and MCL values. The REF-PC and the 0.5nTS-PC samples showed a Q^1/Q^2 value of 1.38 and 1.20, respectively. In addition, the C—S—H MCL values were 5.23 and 4.85, respectively. As commented before, this was probably caused because of the PC addition. The 1nTS-PC sample presented an increase on both Q^1/Q^2 and C—S—H MCL, being 1.67 and 5.86, respectively. According to Kunther *et al.* [70], C—S—H MCL decreases when the Ca/Si ratio is higher than 1.20. They observed that more extended curing periods (as 28 and 91 d) provide a decrease on the MCL even more pronounced when compared to shorter curing periods (7 and 14 d). Moreover, some studies that correlate the C—S—H MCL to compressive strength showed that higher values of MCL indicate high compressive strength [69,70]. Even though the specimens with PC presented a lower MCL value than the others, the compressive strength increased. Nevertheless, among the factors observed through NMR analysis, the w/b ratio was decreased, consequently reducing the pore volume, and increasing the cohesion.

The behavior of nTS during the cement hydration, confirmed using multiple characterization techniques, is schematically summarized in Fig. 11. The good dispersion of nTS favors the increase of C—S—H nucleation sites through the filler effect of nTS core and the reduction of CH content through the pozzolanic reaction of the nTS shell. Therefore, the matrix is denser, and the pore volume and amount are reduced. These effects combined, increase the hydration degree, and lengthen the C—S—H MCL.

Table 3
Deconvoluted ^{29}Si MAS NMR position and percentages.

Mixtures	Chemical shift (ppm) / Q^n relative intensity (%)										α_c (%)	Q^2/Q^1	C—S—H MCL
	Q^0		Q^0(H)		Q^1		Q^2_b		Q^2_p				
REF	−70.68	27.08	−73.08	14.61	−78.53	26.3	−81.06	10.05	−83.98	28.96	41.46	1.48	5.35
05nTS	−70.83	23.25	−72.98	12.77	−78.47	24.54	−81.53	11.92	−83.93	27.53	49.42	1.61	5.70
1nTS	−70.73	18.13	−72.82	12.75	−79.01	26.06	−80.74	12.89	−84.77	30.17	56.64	1.65	5.80
REF-PC	−70.86	30.01	−73.55	14.73	−78.87	23.26	−81.30	11.12	−84.25	20.89	37.18	1.38	5.23
0.5nTS-PC	−70.86	30.01	−73.23	15.24	−78.80	24.88	−81.72	11.09	−83.86	18.79	36.46	1.20	4.85
1nTS-PC	−70.88	25.81	−73.35	12.14	−78.56	23.27	−81.36	12.37	−84.15	26.41	46.71	1.67	5.86

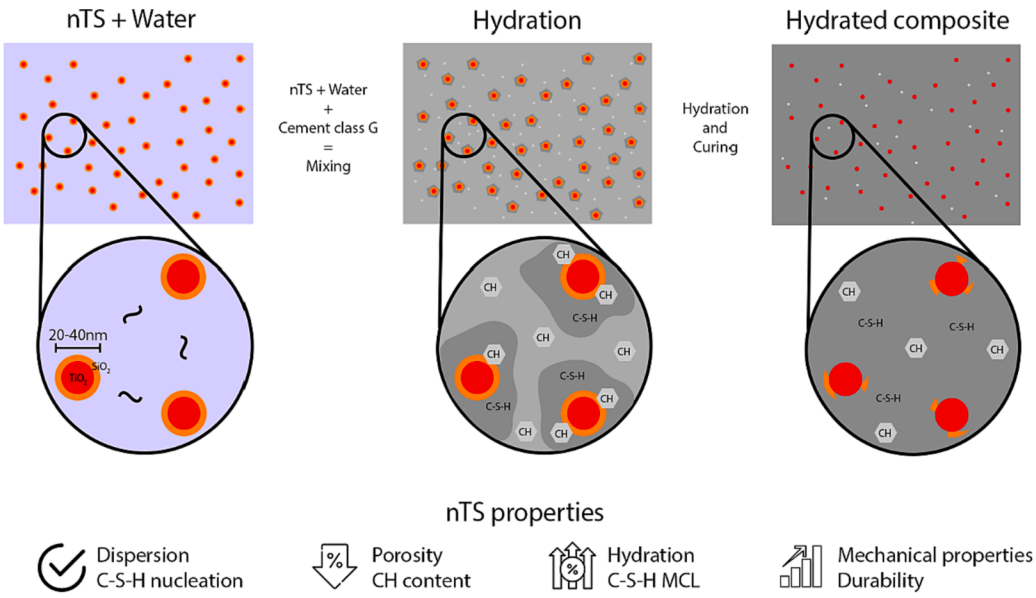

Fig. 11. nTS effect on cement slurry and microstructure.

4. Conclusions

An investigation on nTS addition to oil well cement class G was performed through experimental analysis, and the following conclusions can be taken:

(1) The nTS presented an excellent dispersion in water without any application of dispersive methods. A principle of agglomeration was observed when the w/b was reduced to 0.35, but higher addition amounts should be tested to confirm this behavior.
(2) A much more compact and homogeneous microstructure was obtained when nTS was added. The filler effect and the increase of C—S—H nucleation sites promoted a rise on mechanical properties. The physical advantages, such as higher specific mass and pore refinement were more pronounced with the w/b reduction and in the presence of PC;
(3) The chemical effects endorsed by nTS were very clear and important. The pozzolanic effect reduced the CH content and increased the C—S—H MCL and the hydration degree. These benefits are related to the better physical properties reached with nTS addition;
(4) Although the PC incorporation led to a lower hydration degree and a smaller C—S—H MCL, the PC provides highest compacity and compressive strength, with low pore volume and CH content. The best results were found for the 0.5nTS-PC;
(5) Overall, the nTS provides significant advantages for cement-based materials, specifically oil well cement. Their use combined with PC endorsed important properties, such as self-dispersion, filler and pozzolanic effects, and hydration degree increase. Further investigations are needed to understand its rheological behavior and its resistance against CO_2 acid attack under Carbon Capture and Storage (CCS) conditions.

Suggestions for future studies:

- Evaluate the nTS behavior in cement pastes with PC for longer curing times;
- Increase the addition amount (e.g. 2 and 3 wt%);
- Reduce the w/b ratio and study the hydration degree;
- Study the rheological behavior and hydration rate of the cement slurry;
- Evaluate the hardened cement paste behavior against CO_2 degradation.

CRediT authorship contribution statement

Giovanni dos Santos Batista: Conceptualization, Methodology, Validation, Formal analysis, Investigation, Data curation, Writing – original draft, Writing – review & editing, Visualization. **Antonio Shigueaki Takimi:** Conceptualization, Methodology, Validation, Formal analysis, Writing – original draft, Writing – review & editing. **Eleani Maria da Costa:** Conceptualization, Methodology, Validation, Formal analysis, Writing – original draft, Writing – review & editing, Supervision.

Declaration of Competing Interest

The authors declare that they have no known competing financial interests or personal relationships that could have appeared to influence the work reported in this paper.

Data availability

Data will be made available on request.

Acknowledgments

This work was supported by the Institute of Petroleum and Natural Resources – IPR and The Unit Operations Laboratory – LOPE from PUCRS. This study was partly financed by the Coordenação de Aperfeiçoamento de Pessoal de Nível Superior – Brasil (CAPES) – Finance Code 001.

Appendix A. Supplementary data

Supplementary data to this article can be found online at https://doi.org/10.1016/j.conbuildmat.2022.130282.

References

[1] M.J. Hanus, A.T. Harris, Nanotechnology innovations for the construction industry, Prog. Mater. Sci. 58 (2013) 1056–1102, https://doi.org/10.1016/j.pmatsci.2013.04.001.

[2] F. Pacheco-Torgal, S. Jalali, Nanotechnology: Advantages and drawbacks in the field of construction and building materials, Constr. Build. Mater. 25 (2011) 582–590, https://doi.org/10.1016/j.conbuildmat.2010.07.009.
[3] A.M. Onaizi, G.F. Huseien, N.H.A.S. Lim, M. Amran, M. Samadi, Effect of nanomaterials inclusion on sustainability of cement-based concretes: A comprehensive review, Constr. Build. Mater. 306 (2021), 124850, https://doi.org/10.1016/j.conbuildmat.2021.124850.
[4] B. R., S. J., Effect of Addition of Alccofine on the Compressive Strength of Cement Mortar Cubes, Emerg. Sci. J. 5 (2021) 155–170. doi: 10.28991/esj-2021-01265.
[5] Z. Xu, J. Gao, Y. Zhao, S. Li, Z. Guo, X. Luo, G. Chen, Promoting utilization rate of ground granulated blast furnace slag (GGBS): Incorporation of nanosilica to improve the properties of blended cement containing high volume GGBS, J. Clean. Prod. 332 (2022), 130096, https://doi.org/10.1016/j.jclepro.2021.130096.
[6] Y. Sargam, K. Wang, Quantifying dispersion of nanosilica in hardened cement matrix using a novel SEM-EDS and image analysis-based methodology, Cem. Concr. Res. 147 (2021), 106524, https://doi.org/10.1016/j.cemconres.2021.106524.
[7] B.J. Zhan, D.X. Xuan, C.S. Poon, The effect of nanoalumina on early hydration and mechanical properties of cement pastes, Constr. Build. Mater. 202 (2019) 169–176, https://doi.org/10.1016/j.conbuildmat.2019.01.022.
[8] J. Yuenyongsuwan, S. Sinthupinyo, E.A. O'Rear, T. Pongprayoon, Hydration accelerator and photocatalyst of nanotitanium dioxide synthesized via surfactant-assisted method in cement mortar, Cem. Concr. Compos. 96 (2019) 182–193, https://doi.org/10.1016/j.cemconcomp.2018.11.024.
[9] D. Siang Ng, S.C. Paul, V. Anggraini, S.Y. Kong, T.S. Qureshi, C.R. Rodriguez, Q. Liu, B. Šavija, Influence of SiO2, TiO2 and Fe2O3 nanoparticles on the properties of fly ash blended cement mortars, Constr. Build. Mater. 258 (2020), 119627, https://doi.org/10.1016/j.conbuildmat.2020.119627.
[10] S. Hwang, T. Ozbakkaloglu, S.M. Saleem Kazmi, M.J. Munir, Influence of off-spec fly ash and surfactant-coated nano-iron-oxide on the fresh and hardened properties of cement pastes: An exploratory study, J. Build. Eng. 48 (2022), 103976, https://doi.org/10.1016/j.jobe.2021.103976.
[11] S. Li, Y. Zhang, C. Cheng, H. Wei, S. Du, J. Yan, Surface-treated carbon nanotubes in cement composites: Dispersion, mechanical properties and microstructure, Constr. Build. Mater. 310 (2021), 125262, https://doi.org/10.1016/j.conbuildmat.2021.125262.
[12] E. Karpova, G. Skripkiūnas, I. Barauskas, I. Barauskienė, J. Hodul, Influence of carbon nanotubes and polycarboxylate superplasticiser on the Portland cement hydration process, Constr. Build. Mater. 304 (2021), 124648, https://doi.org/10.1016/j.conbuildmat.2021.124648.
[13] K. Chintalapudi, R.M. Rao Pannem, Strength properties of graphene oxide cement composites, Mater. Today:. Proc. 45 (2021) 3971–3975.
[14] Q. Wang, G. Qi, Y. Wang, H. Zheng, S. Shan, C. Lu, Research progress on the effect of graphene oxide on the properties of cement-based composites, New Carbon Mater. 36 (2021) 729–750, https://doi.org/10.1016/S1872-5805(21)60071-9.
[15] S. Kawashima, K. Wang, R.D. Ferron, J.H. Kim, N. Tregger, S. Shah, A review of the effect of nanoclays on the fresh and hardened properties of cement-based materials, Cem. Concr. Res. 147 (2021), 106502, https://doi.org/10.1016/j.cemconres.2021.106502.
[16] H. Varela, G. Barluenga, I. Palomar, A. Sepulcre, Synergies on rheology and structural build-up of fresh cement pastes with nanoclays, nanosilica and viscosity modifying admixtures, Constr. Build. Mater. 308 (2021), 125097, https://doi.org/10.1016/j.conbuildmat.2021.125097.
[17] M.K. Moraes, E. Maria da Costa, Effect of adding organo-modified montmorillonite nanoclay on the performance of oil-well cement paste in CO2-rich environments, Cem. Concr. Compos. 127 (2022), 104400, https://doi.org/10.1016/j.cemconcomp.2021.104400.
[18] M.T. Alsaba, M.F. Al Dushaishi, A.K. Abbas, A comprehensive review of nanoparticles applications in the oil and gas industry, J. Pet. Explor. Prod. Technol. 10 (4) (2020) 1389–1399.
[19] Z. Zhe, A. Yuxiu, Nanotechnology for the oil and gas industry – an overview of recent progress, Nanotechnol. Rev. 7 (2018) 341–353, https://doi.org/10.1515/ntrev-2018-0061.
[20] J.A. Abdalla, B.S. Thomas, R.A. Hawileh, K.I. Syed Ahmed Kabeer, Influence of nanomaterials on the workability and compressive strength of cement-based concrete, Mater. Today: Proc. 65 (2022) 2073–2076. doi: 10.1016/j.matpr.2022.06.429.
[21] L.P. Singh, S.R. Karade, S.K. Bhattacharyya, M.M. Yousuf, S. Ahalawat, Beneficial role of nanosilica in cement based materials - A review, Constr. Build. Mater. 47 (2013) 1069–1077, https://doi.org/10.1016/j.conbuildmat.2013.05.052.
[22] A.A. Ramezanianpour, M. Mortezaei, S. Mirvalad, Synergic effect of nano-silica and natural pozzolans on transport and mechanical properties of blended cement mortars, J. Build. Eng. 44 (2021), 102667, https://doi.org/10.1016/j.jobe.2021.102667.
[23] G.D.S. Batista, L.B. Schemmer, T.d.A. Siqueira, E.M.d. Costa, Chemical resistance and mechanical properties of nanosilica addition in oil well cement, J. Pet. Sci. Eng. 196 (2021) 107742.
[24] K. Sobolev, I. Flores, L.M. Torres-Martinez, P.L. Valdez, E. Zarazua, E.L. Cuellar, Engineering of SiO2 Nanoparticles for Optimal Performance in Nano Cement-Based Materials, in: Z. Bittnar, P.J.M. Bartos, J. Němeček, V. Šmilauer, J. Zeman (Eds.), Nanotechnology in Construction 3, Springer Berlin Heidelberg, Berlin, Heidelberg, 2009, pp. 139–148.
[25] P. Lawrence, M. Cyr, E. Ringot, Mineral admixtures in mortars, Cem. Concr. Res. 33 (2003) 1939–1947, https://doi.org/10.1016/S0008-8846(03)00183-2.
[26] J.A. Abdalla, B.S. Thomas, R.A. Hawileh, K.I. Syed Ahmed Kabeer, Influence of nanomaterials on the water absorption and chloride penetration of cement-based concrete, Mater. Today: Proc. 65 (2022) 2066–2069. doi: 10.1016/j.matpr.2022.06.427.
[27] J. Chen, S. Kou, C. Poon, Hydration and properties of nano-TiO2 blended cement composites, Cem. Concr. Compos. 34 (2012) 642–649, https://doi.org/10.1016/j.cemconcomp.2012.02.009.
[28] K. Tanaka, M.F.V. Capule, T. Hisanaga, Effect of crystallinity of TiO2 on its photocatalytic action, Chem. Phys. Lett. 187 (1991) 73–76, https://doi.org/10.1016/0009-2614(91)90486-S.
[29] J.A. Abdalla, B.S. Thomas, R.A. Hawileh, J. Yang, B.B. Jindal, E. Ariyachandra, Influence of nano-TiO2, nano-Fe2O3, nanoclay and nano-CaCO3 on the properties of cement/geopolymer concrete, Clean. Mater. 4 (2022), 100061, https://doi.org/10.1016/j.clema.2022.100061.
[30] I. Yurtdas, S.Y. Xie, N. Burlion, J.F. Shao, J. Saint-Marc, A. Garnier, Influence of chemical degradation on mechanical behavior of a petroleum cement paste, Cem. Concr. Res. 41 (2011) 412–421, https://doi.org/10.1016/j.cemconres.2011.01.008.
[31] R.B. Ledesma, N.F. Lopes, K.G. Bacca, M.K.d. Moraes, G.D.S. Batista, M.R. Pires, E. M.d. Costa, Zeolite and fly ash in the composition of oil well cement: Evaluation of degradation by CO2 under geological storage condition, J. Pet. Sci. Eng. 185 (2020) 106656.
[32] M.R. Rostami, F. Abbassi-Sourki, H. Bouhendi, Synergistic effect of branched polymer/nano silica on the microstructures of cement paste and their rheological behaviors, Constr. Build. Mater. 201 (2019) 159–170, https://doi.org/10.1016/j.conbuildmat.2018.12.103.
[33] B. Yuan, Y. Wang, Y. Yang, Y. Xie, Y. Li, Wellbore sealing integrity of nanosilica-latex modified cement in natural gas reservoirs with high H2S contents, Constr. Build. Mater. 192 (2018) 621–632, https://doi.org/10.1016/j.conbuildmat.2018.10.165.
[34] M. Hu, J. Guo, P. Li, D. Chen, Y. Xu, Y. Feng, Y. Yu, H. Zhang, Effect of characteristics of chemical combined of graphene oxide-nanosilica nanocomposite fillers on properties of cement-based materials, Constr. Build. Mater. 225 (2019) 745–753, https://doi.org/10.1016/j.conbuildmat.2019.07.079.
[35] H. Xiao, F. Zhang, R. Liu, R. Zhang, Z. Liu, H. Liu, Effects of pozzolanic and non-pozzolanic nanomaterials on cement-based materials, Constr. Build. Mater. 213 (2019) 1–9, https://doi.org/10.1016/j.conbuildmat.2019.04.057.
[36] B. Han, Z. Li, L. Zhang, S. Zeng, X. Yu, B. Han, J. Ou, Reactive powder concrete reinforced with nano SiO2-coated TiO2, Constr. Build. Mater. 148 (2017) 104–112, https://doi.org/10.1016/j.conbuildmat.2017.05.065.
[37] J. Sun, X. Cao, Z. Xu, Z. Yu, Y. Zhang, G. Hou, X. Shen, Contribution of core/shell TiO2@SiO2 nanoparticles to the hydration of Portland cement, Constr. Build. Mater. 233 (2020), 117127, https://doi.org/10.1016/j.conbuildmat.2019.117127.
[38] API, 10A Specification for Cements and Materials for Well Cementing, 2009.
[39] S.C. Paul, A.S. van Rooyen, G.P.A.G. van Zijl, L.F. Petrik, Properties of cement-based composites using nanoparticles: A comprehensive review, Constr. Build. Mater. 189 (2018) 1019–1034, https://doi.org/10.1016/j.conbuildmat.2018.09.062.
[40] X. Pang, W. Cuello Jimenez, B.J. Iverson, Hydration kinetics modeling of the effect of curing temperature and pressure on the heat evolution of oil well cement, Cem. Concr. Res. 54 (2013) 69–76, https://doi.org/10.1016/j.cemconres.2013.08.014.
[41] A. American Society for Testing and Materials, Standard Test Method For Compressive Strength Of Cylindrical Concrete Specimens - C39/C39M-21, West Conshohocken, PA, USA, 2021.
[42] J. Sun, K. Xu, C. Shi, J. Ma, W. Li, X. Shen, Influence of core/shell TiO2@SiO2 nanoparticles on cement hydration, Constr. Build. Mater. 156 (2017) 114–122, https://doi.org/10.1016/j.conbuildmat.2017.08.124.
[43] D. Koňáková, V. Pommer, K. Šádková, M. Keppert, R. Černý, E. Vejmelková, Impact of plasticizers' types on the performance of calcium aluminate cement, J. Mater. Res. Technol. 20 (2022) 1512–1523, https://doi.org/10.1016/j.jmrt.2022.07.155.
[44] M.H.R. Khudair, M.S. Elyoubi, A. Elharfi, Study of the influence of water reducing and setting retarder admixtures of polycarboxylate "s uperplasticizers " on physical and mechanical properties of mortar and concrete, J. Mater. Environ. Sci. 9 (2018) 56–65, https://doi.org/10.26872/jmes.2018.9.1.7.
[45] P.K. Mehta, P.J.M. Monteiro, Concrete: Microstructure, Properties and Materials, fourth, McGraw Hill Professional, Berkeley, 2013.
[46] R.J. Gao, S.H. Lv, Q. Cao, Effects of Polycarboxylate Superplasticizers on Hydration and Microstructure of Hardened Cement Paste, Adv. Mat. Res. 487 (2012) 692–696, https://doi.org/10.4028/www.scientific.net/AMR.487.692.
[47] V. Morin, F. Cohen Tenoudji, A. Feylessoufi, P. Richard, Superplasticizer effects on setting and structuration mechanisms of ultrahigh-performance concrete, Cem. Concr. Res. 31 (2001) 63–71, https://doi.org/10.1016/S0008-8846(00)00428-2.
[48] F. Kong, L. Pan, C. Wang, D. Zhang, N. Xu, Effects of polycarboxylate superplasticizers with different molecular structure on the hydration behavior of cement paste, Constr. Build. Mater. 105 (2016) 545–553, https://doi.org/10.1016/j.conbuildmat.2015.12.178.
[49] V.H.J.M.D. Santos, D. Pontin, G.G.D. Ponzi, A.S.d.G.e. Stepanha, R.B. Martel, M. K. Schütz, S.M.O. Einloft, F. Dalla Vecchia, Application of Fourier Transform infrared spectroscopy (FTIR) coupled with multivariate regression for calcium carbonate (CaCO3) quantification in cement, Constr. Build. Mater. 313 (2021) 125413.
[50] F. Winnefeld, S. Becker, J. Pakusch, T. Götz, Effects of the molecular architecture of comb-shaped superplasticizers on their performance in cementitious systems, Cem. Concr. Compos. 29 (2007) 251–262, https://doi.org/10.1016/j.cemconcomp.2006.12.006.
[51] S. Ng, H. Justnes, Influence of plasticizers on the rheology and early heat of hydration of blended cements with high content of fly ash, Cem. Concr. Compos. 65 (2016) 41–54, https://doi.org/10.1016/j.cemconcomp.2015.10.005.

[52] B. Lothenbach, F. Winnefeld, R. Figi, The influence of superplasticizers on the hydration of Portland cement, in: 12th International Congress on the Chemistry of Cement, Montreal, Canada, 2007.
[53] M.-E.-S.-I. Saraya, Study physico-chemical properties of blended cements containing fixed amount of silica fume, blast furnace slag, basalt and limestone, a comparative study, Constr. Build. Mater. 72 (2014) 104–112, https://doi.org/10.1016/j.conbuildmat.2014.08.071.
[54] P. Yu, R.J. Kirkpatrick, B. Poe, P.F. McMillan, X. Cong, Structure of Calcium Silicate Hydrate (C-S-H): Near-, Mid-, and Far-Infrared Spectroscopy, J. Am. Ceram. Soc. 82 (2004) 742–748, https://doi.org/10.1111/j.1151-2916.1999.tb01826.x.
[55] T. Richard, L. Mercury, F. Poulet, L. d'Hendecourt, Diffuse reflectance infrared Fourier transform spectroscopy as a tool to characterise water in adsorption/confinement situations, J. Colloid Interface Sci. 304 (2006) 125–136, https://doi.org/10.1016/j.jcis.2006.08.036.
[56] M.A. Trezza, A.E. Lavat, Analysis of the system 3CaO·Al2O3–CaSO4·2H2O–CaCO3–H2O by FT-IR spectroscopy, Cem. Concr. Res. 31 (2001) 869–872, https://doi.org/10.1016/S0008-8846(01)00502-6.
[57] C. Gabrielli, R. Jaouhari, S. Joiret, G. Maurin, In situ Raman spectroscopy applied to electrochemical scaling. Determination of the structure of vaterite, J. Raman Spectrosc. 31 (2000) 497–501, https://doi.org/10.1002/1097-4555(200006)31:6<497::AID-JRS563>3.0.CO;2-9.
[58] A. Hidalgo, S. Petit, C. Domingo, C. Alonso, C. Andrade, Microstructural characterization of leaching effects in cement pastes due to neutralisation of their alkaline nature, Cem. Concr. Res. 37 (2007) 63–70, https://doi.org/10.1016/j.cemconres.2006.10.002.
[59] R. Ylmén, U. Jäglid, B.-M. Steenari, I. Panas, Early hydration and setting of Portland cement monitored by IR, SEM and Vicat techniques, Cem. Concr. Res. 39 (2009) 433–439, https://doi.org/10.1016/j.cemconres.2009.01.017.
[60] I. Aiad, A.M. Al-Sabagh, S.H. Shafek, A.I. Adawy, S.A. Abo-EL-Enein, Effect of some prepared superplasticizers (Cyclohexanone Based) on compressive strength and physico-chemical properties of oil well cement pastes, Egypt. J. Pet. 26 (2017) 843–850, https://doi.org/10.1016/j.ejpe.2016.10.019.
[61] M. Li, M. Liu, Y. Yang, Z. Li, X. Guo, Mechanical properties of oil well cement stone reinforced with hybrid fiber of calcium carbonate whisker and carbon fiber, Pet. Explor. Dev. 42 (2015) 104–111, https://doi.org/10.1016/S1876-3804(15)60012-X.
[62] M.S. Amin, A.O. Habib, S.A. Abo-El-Enein, Hydrothermal characteristics of high-slag cement pastes made with and without silica sand, Adv. Cem. Res. 24 (2012) 23–31, https://doi.org/10.1680/adcr.2012.24.1.23.
[63] M.S. Morsy, A.F. Galal, S.A. Abo-El-Enein, Effect of temperature on phase composition and microstructure of artificial pozzolana-cement pastes containing burnt kaolinite clay, Cem. Concr. Res. 28 (1998) 1157–1163, https://doi.org/10.1016/S0008-8846(98)00083-0.
[64] X. Pang, L. Sun, M. Chen, M. Xian, G. Cheng, Y. Liu, J. Qin, Influence of curing temperature on the hydration and strength development of Class G Portland cement, Cem. Concr. Res. 156 (2022), 106776, https://doi.org/10.1016/j.cemconres.2022.106776.
[65] A. Bajza, I. Rouseková, Effect of heat treatment conditions on the pore structure of cement mortars, Cem. Concr. Res. 13 (1983) 747–750, https://doi.org/10.1016/0008-8846(83)90067-4.
[66] C.J. Fordham, I.J. Smalley, A simple thermogravimetric study of hydrated cement, Cem. Concr. Res. 15 (1985) 141–144, https://doi.org/10.1016/0008-8846(85)90019-5.
[67] M.D. Andersen, H.J. Jakobsen, J. Skibsted, Characterization of white Portland cement hydration and the C-S-H structure in the presence of sodium aluminate by 27Al and 29Si MAS NMR spectroscopy, Cem. Concr. Res. 34 (2004) 857–868, https://doi.org/10.1016/j.cemconres.2003.10.009.
[68] I. Garcia-Lodeiro, G. Goracci, J.S. Dolado, M.T. Blanco-Varela, Mineralogical and microstructural alterations in a portland cement paste after an accelerated decalcification process, Cem. Concr. Res. 140 (2021), 106312, https://doi.org/10.1016/j.cemconres.2020.106312.
[69] J.J. Kim, E.M. Foley, M.M. Reda Taha, Nano-mechanical characterization of synthetic calcium–silicate–hydrate (C–S–H) with varying CaO/SiO2 mixture ratios, Cem. Concr. Compos. 36 (2013) 65–70, https://doi.org/10.1016/j.cemconcomp.2012.10.001.
[70] W. Kunther, S. Ferreiro, J. Skibsted, Influence of the Ca/Si ratio on the compressive strength of cementitious calcium–silicate–hydrate binders, J. Mater. Chem. A Mater. 5 (2017) 17401–17412, https://doi.org/10.1039/C7TA06104H.